RSC Advances

PAPER

Cite this: *RSC Adv.*, 2023, **13**, 23690

A novel "turn-off" photoelectrochemical aptasensing platform for selective detection of tobramycin based on the Ti_3C_2–MoS_2/BiOI heterojunction†

Xuejun Qi * and Xing Zhao

Received 17th July 2023
Accepted 28th July 2023

DOI: 10.1039/d3ra04800d

rsc.li/rsc-advances

Tobramycin (TOB), as a widely used antibiotic, poses severe unpredictable risks to ecology and health. In this study, a novel photoelectrochemical (PEC) adapter sensor, based on its "turn-off" PEC mode, was constructed for TOB detection. This visible-light-driven photoelectrochemical (PEC) aptasensor was successfully developed for TOB detection using Ti_3C_2–MoS_2/BiOI and TOB aptamer probes. When TOB was captured by probes anchored on the modified electrode, a decreased photocurrent was also noted due to steric hindrance and this further hindered electron transfer. Under optimal conditions, 0.001 ng mL^{-1} to 40 ng mL^{-1} of TOB could be identified, with the detection limit being as low as 0.5 pg mL^{-1}. At the same time, actual samples were also explored. Finally, the proposed sensor exhibited high specificity, satisfactory detectability and great reproducibility, thereby providing a novel approach for the detection of pollutants.

1. Introduction

Tobramycin (TOB) is an aminoglycoside antibiotic that displays bactericidal activity against different types of bacteria, especially *Pseudomonas aeruginosa*.[1] However, it is a particularly toxic chemical that persists in the aquatic environment, with even trace amounts likely to cause damage to kidney and liver cells.[2,3] Therefore, it is essential to check for the presence of TOB and to treat effluents accordingly in order to conform to environmental regulations.[4] In this context, various techniques, including sensitive surface-enhanced Raman spectroscopy (SERS),[5] fluorescent,[6] and electrochemical[7] have been applied so far for detecting pollutants in aquatic systems.

In recent years, photoelectrochemical (PEC) biosensors have become a research hotspot as an alternative analytical approach due to their low phototoxicity, minimum photobleaching and minimum biomolecular photodamage.[8,9] When constructing PEC sensors, their sensitivity is usually improved by enhancing the performance of photocatalysts.[10] However, at the same time, PEC sensing is also conducted based on non-analyte-specific photocatalytic reactions, and to overcome this issue, there is a need to improve the selectivity of PEC sensors through the introduction of different recognition elements.[11,12] Among these, aptamers represent well-recognized antibody mimetics that can specifically recognize targets, and as such, they are widely adopted for constructing PEC aptasensors that can display high selectivity towards analytes such as proteins, inorganic ions, antibiotics, cells as well as organic compounds.[13–15]

In addition, it can be challenging to develop semiconductor-based materials for PEC sensors of high sensitivity and selectivity, but various semiconducting materials have now been synthesized for this purpose.[16] For instance, bismuth-based nanocomposites (BiOX, $BiWO_4$, $BiPO_4$ and $BiVO_4$) have attracted attention for sensing and catalytic applications.[17,18] BiOI displays a layered structure, consisting of a layer of $[Bi_2O_2]^{2+}$ as well as double layers of iodine ions, with internal static electric fields connecting the two.[19] This unique layered structure is actually advantageous for the separation of photogenerated electron–hole pairs.[20] As such, BiOI is considered to be one of the most promising photocatalysts owing to its good photocatalytic activity under visible light.[21]

BiOI has also attracted interest for applications in water decontamination as it is non-toxic, of low cost and environmentally friendly.[22] However, the photocatalytic activity of BiOI is still slightly low, thus limiting its practical uses.[23] Therefore, to overcome this challenge, there have been proposals to apply technologies such as doping diverse metals, using metal oxides or generating heterojunctions with additional semiconductors.[24,25] Of those modification approaches, constructing heterojunctions with diverse semiconductors was actually shown to be efficient, and in this context, great attention has been paid to sulfide-based materials (CdS, CuS, MoS_2 and ZnS),

---

School of Architecture and Civil Engineering, Xihua University, Chengdu 610039, PR China. E-mail: xuejunqi@hotmail.com

† Electronic supplementary information (ESI) available. See DOI: https://doi.org/10.1039/d3ra04800d

because of the ease with which they absorb light as well as their narrow band gap.[26,27] In particular, MoS_2 has good photocatalytic performance due to the special sandwich layered structure of the S–Mo–S atoms, while at the same time, it is characterized by a narrow band gap, a large absorption coefficient and is easily prepared. These features suggest that MoS_2 has great potential in the field of photocatalysis.[28] In fact, coupling BiOI with a narrow band gap semiconductor such as MoS_2 may broaden the absorption range and suppress electron–hole pairs recombination, thereby improving the photocatalytic and photoelectrochemical activity of BiOI.

MXenes, a new type of two-dimensional transition metal carbide/carbonitride, have attracted attention as a result of their high electrical conductivity and reactivity, their large specific surface area as well as their structure stability.[29] One example is Ti_3C_2 for which the unique two-dimensional structure, with its large number of –O terminals, is useful to build heterojunctions based on Ti_3C_2 and other semiconductors. This is often achieved through electrostatic adsorption which not only establishes a strong contact between the Ti_3C_2 and semiconductors, but also allows the former to serve as cocatalysts in the heterojunction.[30] However, its high anisotropic carrier (electron and hole) mobility and outstanding metallic conductivity can also promote the separation and migration of photogenerated charges. Nevertheless, to the best of the authors' knowledge, there are only few reports on the application of Ti_3C_2 as an auxiliary agent to boost the efficiency of semiconductors' charge transfer for PEC-based detection of antibiotic molecules.[31]

Based on the above, a Ti_3C_2–MoS_2/BiOI heterojunction catalyst was prepared *via* a simple method. Ti_3C_2- and MoS_2-modified BiOI improved the light absorption capacity, surpassing those of MoS_2 and BiOI alone while demonstrating that BiOI, modified with the two compounds, could promote photogenerated electron–hole pair separation and boost photo-to-current efficiency. The superior Ti_3C_2–MoS_2/BiOI photoactive material was also found to be a successful PEC aptasensor for TOB detection as it offered an extensive linear range and low detection limit. In addition, the findings further suggested that Ti_3C_2–MoS_2/BiOI nanocomposites could be potentially used in fields for PEC-based sensing as well as photocatalysis.

2. Experiment

In this study, the materials, apparatus and material synthesis steps are presented in ESI.†

2.1. Construction of PEC aptasensor

Before preparation, we cleaned indium tin oxide (ITO, 1 cm × 2 cm) electrode using 0.1 M NaOH solution before sonication within ultrapure water and subsequent ethanol. The electrode was later subjected to drying in the presence of infrared light. We synthesized PEC aptasensor as follows. First of all, this study modified Ti_3C_2–MoS_2/BiOI suspension (20 μL) with ITO in the fixed geometric region (0.5 cm × 1 cm), followed by drying at ambient temperature for forming the Ti_3C_2–MoS_2/BiOI electrode. Afterwards, 20 μL of 3 μM TOB aptamer solution was added to the Ti_3C_2–MoS_2/BiOI surface and incubated overnight at 4 °C. When not used, the obtained sensor was stored at 4 °C.

2.2. Electrochemical experiments

Experimenters implemented electrochemical experiments on a CHI 660E electrochemical workstation equipped with a three-electrode system. Pt wire was used as the counter electrode, saturated calomel electrode (SCE) as the reference electrode, and ITO glass as the working electrode. The light source came from a xenon lamp (PLS-SXE 300, 100 mW cm^{-2}, $\lambda \geq 420$ nm) and the light source was kept at 15 cm while the modified electrode was applied in the PEC system to detect TOB at an operating potential of 0.1 V. Electrochemical impedance spectroscopy (EIS) was performed in PBS (0.1 M, pH = 7). To investigate the detection performance of PEC aptasensor, the prepared aptamer/Ti_3C_2–MoS_2/BiOI electrode was incubated with 20 μL of TOB solution at various concentrations for 40 min.

3. Results and discussion

3.1. Detection principle of the PEC aptasensor

In the presence of visible radiation, MoS_2 could absorb photons and generate electron–hole pairs, the holes of the valence band (VB) in MoS_2, that participated in redox reaction. In this case, the electrons of the conduction band (CB) could be easily transferred into the CB of BiOI and pass *via* the circuit to generate the photocurrent.[32] Since the work function of Ti_3C_2 was lower than that of BiOI, the photogenerated electrons in BiOI across the 'upward' bent CB at the BiOI/Ti_3C_2 interface could be transferred to Ti_3C_2. Moreover, a Schottky junction was formed by the different Fermi levels of BiOI and metallic Ti_3C_2, with these suppressing the charge diffusion from Ti_3C_2 to BiOI. In addition, due to the introduction of Ti_3C_2, the enhanced photocurrent response could be caused by the promotion of charge separation by the strong visible light adsorption. A subsequent "turn-off" signal response mode would then be opened owing to the switch of steric hindrance from the specific capturing TOB by the aptamer probes on the Ti_3C_2–MoS_2/BiOI surface. Therefore, an ultrasensitive detection of TOB was achieved by the proposed PEC aptasensor owing to the excellent photoelectric properties of the prepared composites as well as the specific recognition feature of aptamer probes (Scheme 1).[1,9]

3.2. Characterization of the materials

Fig. 1A shows the XRD patterns of the prepared samples. The diffraction peaks of MoS_2 at 12.6°, 31.2° and 34.6° corresponded to the (002), (100), (102) crystal plane, thus revealing the anatase phase of MoS_2 (JCPDS No. 37-1492). Regarding the pattern for BiOI, there were peaks at 29.64°, 31.66°, 45.67° and 55.15° which could be assigned to (102), (110), (104) and (212) crystal planes, and these results suggested that BiOI belongs to a monoclinic crystal (JCPDS 10-0445). In the case of MoS_2/BiOI-6%, characteristic peaks of both MoS_2 and BiOI occurred simultaneously, hence indicating that the MoS_2 was successfully loaded onto the BiOI nanosheets. Similarly, since the characteristic peaks of Ti_3C_2 were also retained in Ti_3C_2–MoS_2/

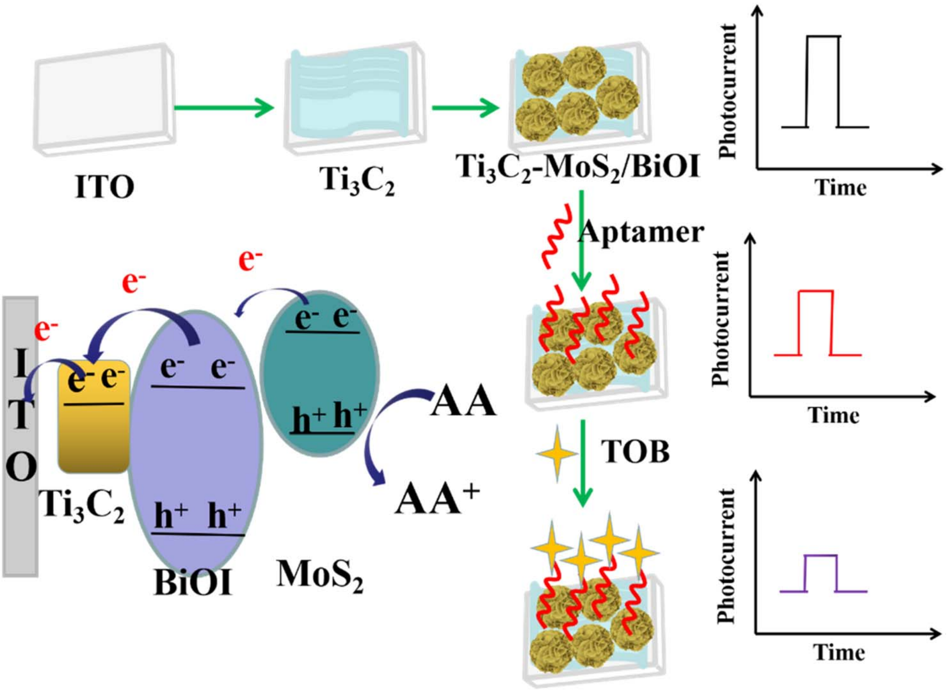

Scheme 1 Preparation of the PEC sensor for TOB detection under light irradiation.

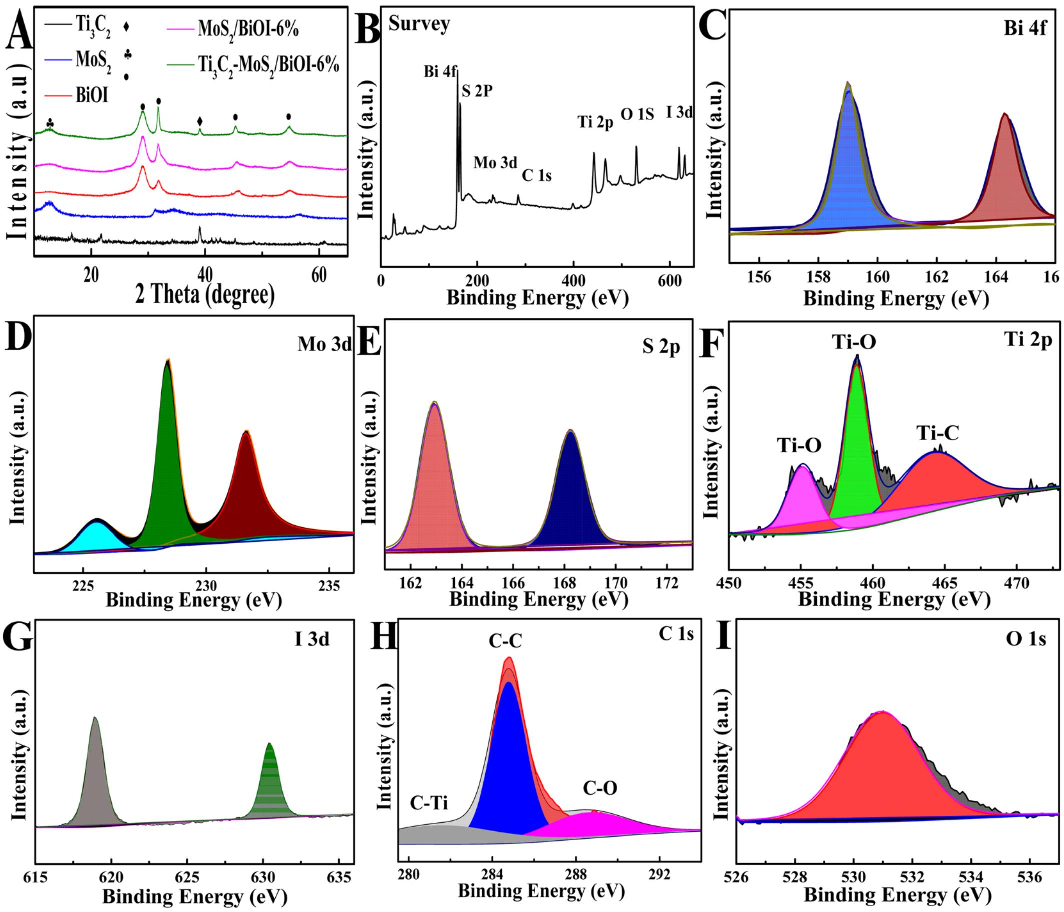

Fig. 1 (A) XRD spectra of BiOI, Ti_3C_2, MoS_2, MoS_2/BiOI-6% and Ti_3C_2–MoS_2/BiOI-6% composites; XPS of (B) survey, (C) Bi 4f, (D) Mo 3d, (E) S 2p, (F) Ti 2p, (G) I 3d, (H) C 1s and (I) O 1s.

BiOI-6%, this was an indication that the crystal structure had not changed. Therefore, based on the results, it could be inferred that the "accordion" structure of Ti_3C_2 was not destroyed after the introduction of MoS_2/BiOI, with the latter deposited onto the surface of Ti_3C_2.

XPS was also conducted to analyze the surface electronic state as well as the chemical composition of Ti_3C_2–MoS_2/BiOI-6%. As revealed by the XPS spectrum (Fig. 1B), O, Bi, Mo, I, Ti, C and S elements were all distributed within the composites. More specifically, two 4f binding energies were observed (Fig. 1C) at 159.25 and 164.55 eV for Bi, and they were respectively associated with Bi $4f_{7/2}$ and Bi $4f_{5/2}$ in standard Bi^{3+}.[33] Similarly, Mo $3d_{3/2}$ at 231.6 eV and Mo $3d_{5/2}$ at 228.4 eV were matched to Mo^{4+},[34] as shown in Fig. 1D, while in the case of the 2p spectra of S, binding energies for both diverse phases could be observed (Fig. 1E), with 161.6 and 163.1 eV being associated with S $2p_{3/2}$ and S $2p_{1/2}$ of MoS_2, respectively.[35] Regarding Ti_3C_2, high-resolution 2p spectra of Ti featured three peaks (Fig. 1F); the peak at 455.2 was associated with Ti–C, while those detected at 458.9 and 464.6 eV were assigned to Ti–O, as a result of sufficient hydrophilic functional groups (–OH, –O) following HF etching.[36] Two peaks, corresponding to $3d_{3/2}$ (630.2 eV) and $3d_{5/2}$ (618.5 eV) in biological iodine, were further associated with I^{-1} (Fig. 1G),[33] while the C 1s peaks (Fig. 1H) at 288.9, 284.7, and 281.5 eV could be assigned to C–O, C–C and Ti–C, respectively. Finally, peaks detected at 530.61 eV for O 1s (Fig. 1I) were associated with BiOI.[30] Overall, the results showed that the complex consisted of Ti_3C_2, MoS_2 and BiOI.

SEM analysis was subsequently applied to determine the morphology of the materials. In this case, the topical multilayer accordion-like nanostructure of Ti_3C_2 could be clearly observed (Fig. 2A), and at the same time, MoS_2/BiOCl hierarchical microspheres can *in situ* grow onto the surface of Ti_3C_2 (Fig. 2B). And MoS_2/BiOCl presented a large number of sheet-shaped structures that were nearly 2 μm in length (inset of Fig. 2B), TEM and HRTEM were then used to characterize the morphology of Ti_3C_2 (Fig. 2C) and Ti_3C_2–MoS_2/BiOI-6% (Fig. 2D), with the hierarchical microspheres of MoS_2/BiOI found to adhere closely to the Ti_3C_2 surface (inset of Fig. 2D). The element mapping images (Fig. 2E–K) confirm that the existence and distribution of Ti, C, O, S, Bi, I, and Mo elements in the Ti_3C_2–MoS_2/BiOI-6% composite.

The above characterization was followed by ultraviolet visible diffused reflectance spectra (UV-vis DRS) for analyzing the absorbance properties of the composites. As shown in Fig. 3A, BiOI displayed a strong absorption within the range of 200–500 nm. However, both MoS_2/BiOI-6% and Ti_3C_2–MoS_2/BiOI-6% presented a significantly enhanced visible light absorption compared with that of the BiOI, hence revealing their superior optical properties. Based on the basic electronegativity concept,[37] the band gap energy was then computed using eqn (1).

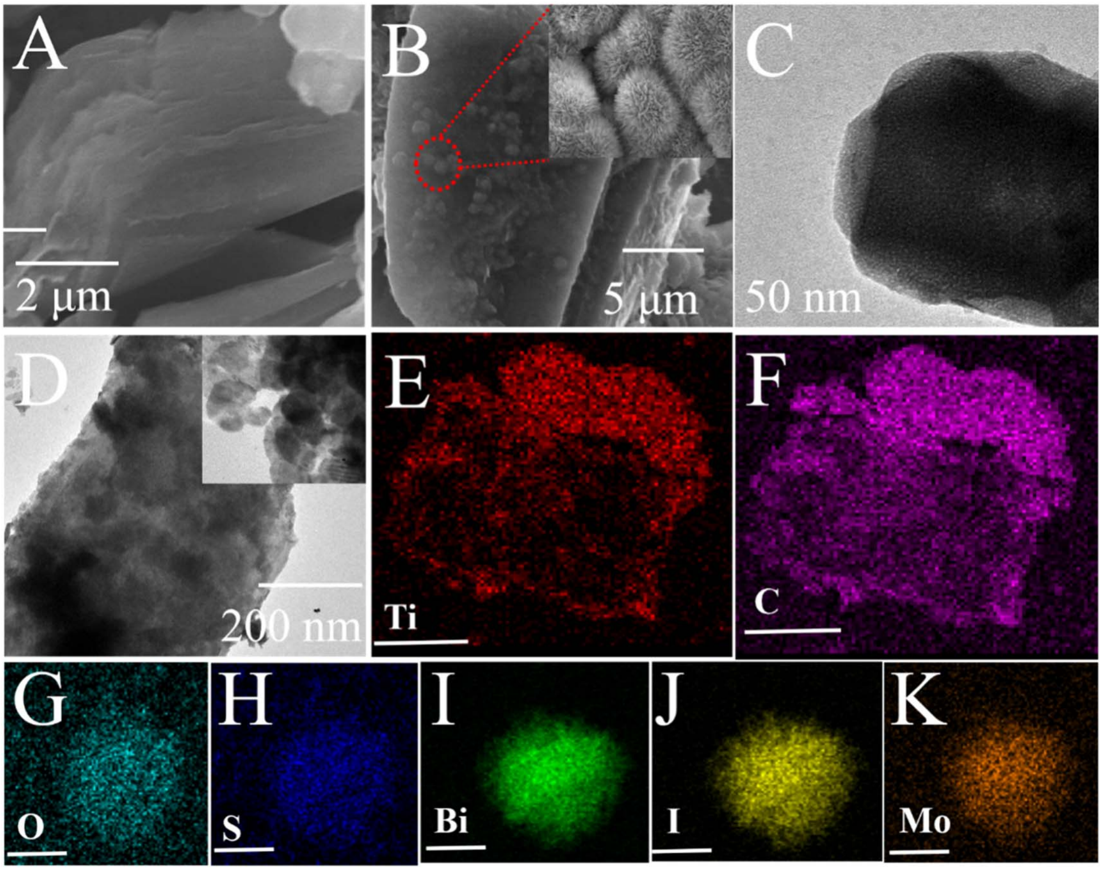

Fig. 2 SEM and TEM images of Ti_3C_2 (A) and (C) and Ti_3C_2–MoS_2/BiOI-6% (B) and (D), elemental mapping of Ti_3C_2–MoS_2/BiOI-6% (E)–(K).

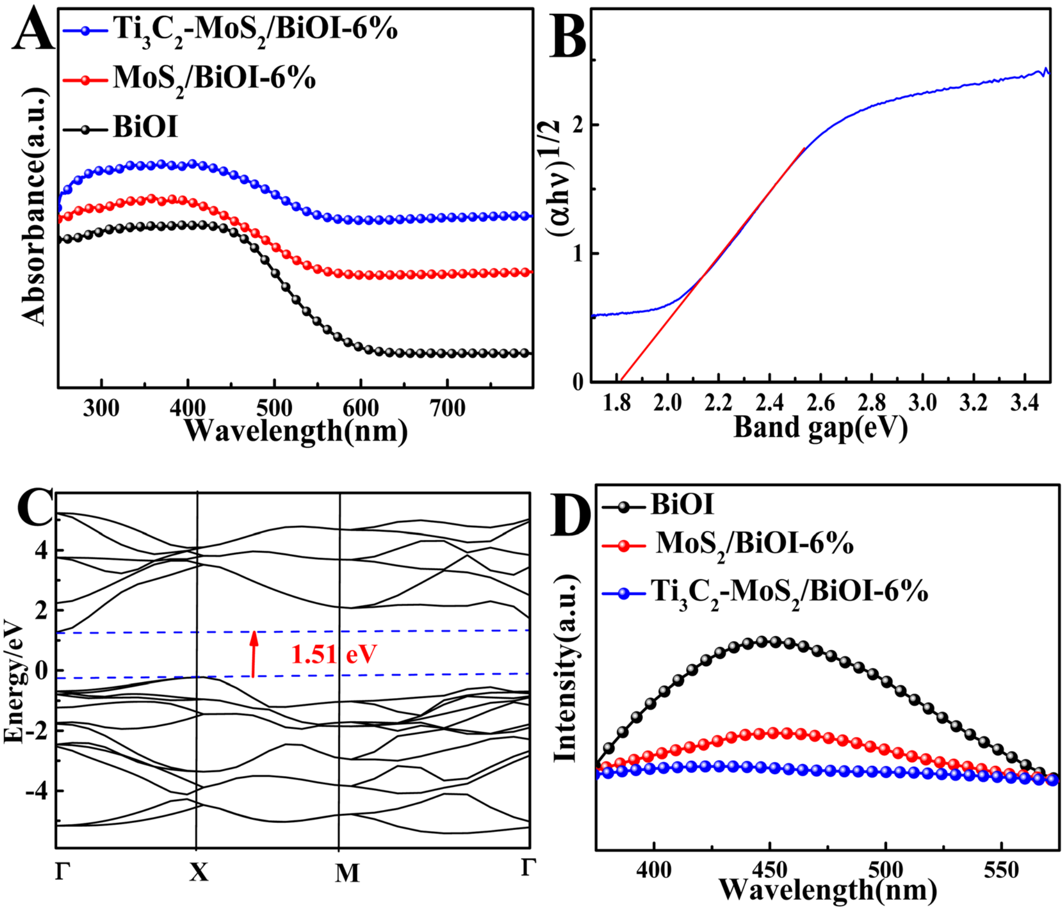

Fig. 3 UV-vis diffuse reflectance spectra (A) of BiOI, MoS_2/BiOI-6% and Ti_3C_2–MoS_2/BiOI-6%; (B) plots of $(Ah\nu)^{1/n}$ *vs.* photon energy ($h\nu$); (C) band structures of BiOI; PL spectra (D) of BiOI, MoS_2/BiOI-6% and Ti_3C_2–MoS_2/BiOI-6%.

$$\alpha h\nu = A(\nu h - E_g)^{n/2} \qquad (1)$$

where A is the absorption coefficient, h is the Planck's constant, ν is the incident light frequency, A is a constant, and n is the type of optical transition. With BiOI being an indirect semiconductor, the value of n was 1. The E_g gap energy of BiOI is 1.79 eV (Fig. 3B). DFT determined energy band structures for BiOI (Fig. 3C). Clearly, BiOI acted as the photocatalytic material of an indirect band-gap semiconductor since the valence band maximum (VBM) and conduction band minimum (CBM) were positioned at diverse high symmetry points, as observed by the CBM at the Γ-point and VBM at the X-point. Using the above equation, a BiOI band gap of 1.51 eV was obtained. Apparently, the band gaps were notably lower compared with experimental measurements, probably due to the defected GGA function.[36]

Moreover, the separation and recombination rates of photoexcited charge carriers were explored using photoluminescence (PL) spectra. In this case, the Ti_3C_2–MoS_2/BiOI-6% showed the weakest emission peak intensity (Fig. 3D). These results not only indicated the lowest recombination rate for photoinduced charge carriers, but also an excellent electron and hole behavior, thus demonstrating the composite's practical value for the development of sensitive PEC sensors.[38]

3.3. Characterization of the PEC aptasensor

Fig. 4A presents the photocurrent densities during various measures taken for the PEC aptasensor, with that of BiOI being a small value. In contrast, the photocurrent density of MoS_2/BiOI-6% was significantly higher at 3.59 μA cm^{-2}, hence indicating that the combination of MoS_2 with BiOI could promote the migration of photoinduced electrons to significantly enhance the photocurrent response of the composites. EIS was adopted for investigating the construction of PEC sensors (Fig. 4B). All EIS data were applied using an equivalent circuit model, including the electrolyte resistance (R_s), the double-layer capacitance (C_{dl}), the charge transfer resistance (R_{ct}) as well as the Warburg impedance (Z_w). Initially, the EIS of BiOI was measured and it displayed a semicircle of large diameter. More specifically, the EIS value was approximately 206.3 Ω, while that of MoS_2/BiOI-6% decreased to 188.4 Ω. In addition, the impedance value also showed an obvious decrease to 162.9 Ω after the introduction of Ti_3C_2.[32]

The photocurrent density also decreased gradually compared with Ti_3C_2–MoS_2/BiOI-6% after adding the aptamer (Fig. 5A), as the electron exchange with the electrode surface of Ti_3C_2–MoS_2/BiOI-6% as well as the electron donor of ascorbic acid (AA) were impeded. Furthermore, when TOB was

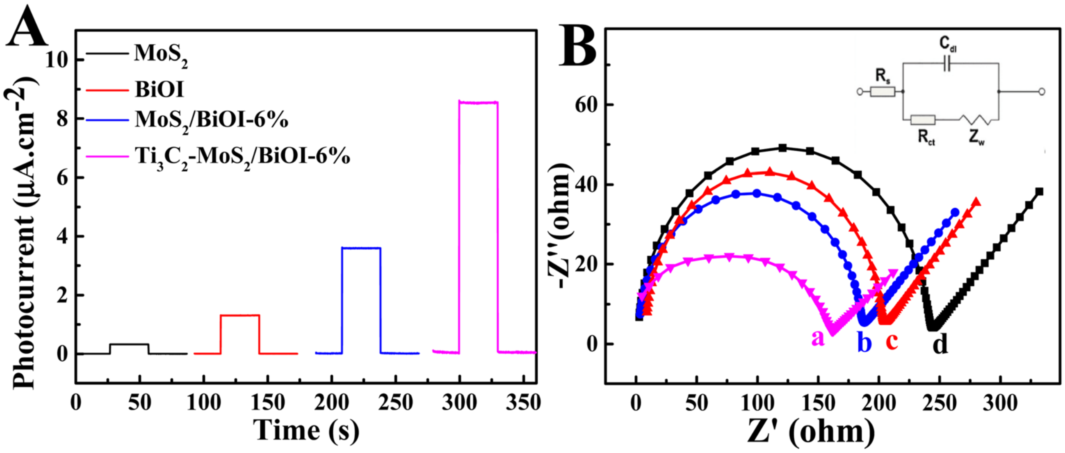

Fig. 4 Photocurrent responses in PBS (A) and EIS spectra (B) at a bias potential of 0.1 V in 0.1 M of KCl containing 5 mM $[Fe(CN)_6]^{3-/4-}$ of the materials Ti_3C_2–MoS_2/BiOI-6% (a), MoS_2/BiOI-6% (b), BiOI (c) and MoS_2 (d).

supplemented, the strong binding ability and high affinity of aptamer molecules to TOB resulted in the formation of a large amount of poorly conductive TOB–aptamer complexes, with the latter usually formed by capturing TOB onto the sensing interface to increase electron transfer resistance as well as lower the photocurrent density. Therefore, changes in photocurrent density can also be adopted for quantifying TOB. The results revealed that the reduced photocurrent density could be the

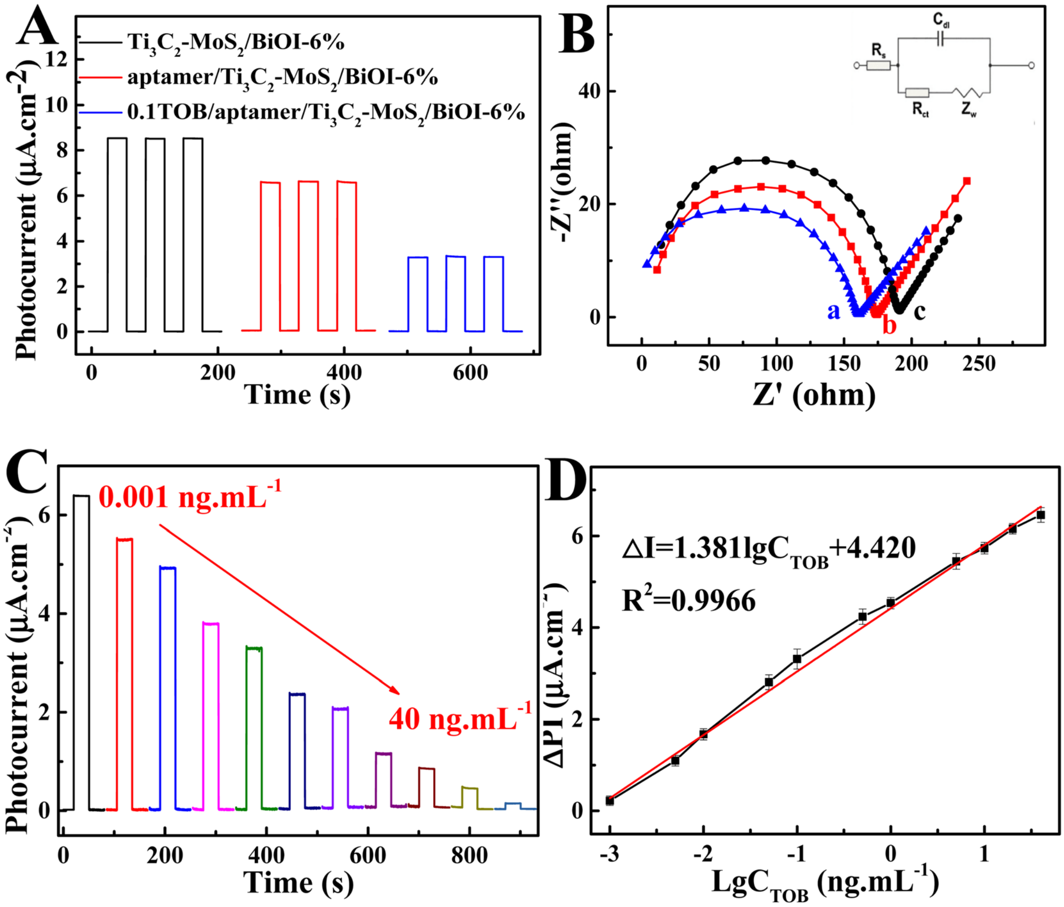

Fig. 5 Photocurrent responses in PBS (A) and EIS spectra (B) at a bias potential of 0.1 V in 0.1 M of KCl containing 5 mM $[Fe(CN)_6]^{3-/4-}$ of the materials Ti_3C_2–MoS_2/BiOI-6% (a), aptamer/Ti_3C_2–MoS_2/BiOI-6% (b) and TOB/aptamer/Ti_3C_2–MoS_2/BiOI-6% (c); (C) photocurrent responses of the aptamer/Ti_3C_2–MoS_2/BiOI-6% at various TOB levels in PBS (0.1 M, pH 7.0) at a bias potential of 0.1 V: (0.001–40 ng mL^{-1}); (D) the linear calibration curve for TOB determination.

result of a recognition reaction between aptamer and TOB, and based on this, a detection mechanism of the PEC aptasensor for TOB could then be put forward. The EIS value increased again to 174.6 Ω with the aptamer being anchored on the surface of Ti_3C_2–MoS_2/BiOI-6% (Fig. 5B). This could be due to the fact that aptamers can increasingly hinder electron transfer. Besides, after the incubation of the PEC aptasensor with TOB, the EIS value further increased to 191.3 Ω. This could be attributed to the formation of TOB–aptamer complexes of poor conductivity as they inhibit the electron transfer between the sensing interface and the solution. Moreover, the findings of the EIS characterization were consistent with those of PEC characterization, thereby suggesting that the preparation of PEC aptasensors was successfully achieved.

3.4. Performance of the PEC aptasensor

In accordance with best experimental conditions, a PEC biosensor for detecting TOB was constructed using the direct relationship between the photocurrent of a biosensor and the concentration of TOB. As shown in Fig. 5C, when the concentration of the target TOB increased from 0.001 ng mL^{-1} to 40 ng mL^{-1}, photocurrent responses of the biosensor decreased progressively. Fig. 5D further presents the good linear correlation between the logarithm of TOB concentration and photocurrent response, with the linear regression equation being ΔPI $(\mu A\ cm^{-2}) = 1.381 \lg C\ (ng\ mL^{-1}) + 4.420$ $(R = 0.9966)$. Moreover, the biosensor showed an acceptable detection limit of 0.5 pg mL^{-1}. In comparison with other existing biosensors (Table S1†), the one under study therefore displayed good results in a linear range, repeatability, long-term stability and incubation time, amongst others.

Selectivity represents a vital detection index for aptasensors, and it is studied by measuring the current change of the aptasensor to other intermediate substances (Fig. 6A). The photocurrent showed obvious changes after adding TOB (0.1 ng mL^{-1}), but when five different interfering agents (5 ng mL^{-1}) were added, the photocurrent was exactly the same as that of the blank sample, thereby indicating that the sensor had high TOB selectivity. Five Ti_3C_2–MoS_2/BiOI-6% electrodes were subsequently prepared under similar conditions to explore the aptasensor's reproducibility (Fig. S3A†). In this case, the results showed great reproducibility, with the relative standard deviation (RSD) of five independent measurements being only 2%. Moreover, the findings further demonstrated the great long-term stability of the designed PEC aptasensors. Indeed, as shown in Fig. S3B,† after 500 s of light–dark alternating cycles measured with *i*–*t*, the dark current and photocurrent of the selfsensor remained almost unchanged. At the same time, the photocurrent of the last cycle to be assessed was still at 98.8% of the first cycle, suggesting that the PEC adaptive sensor had good stability. Finally, the shelf-life of the PEC aptasensor was also examined. Fig. 6B shows the PEC signal of the Ti_3C_2–MoS_2/BiOI-

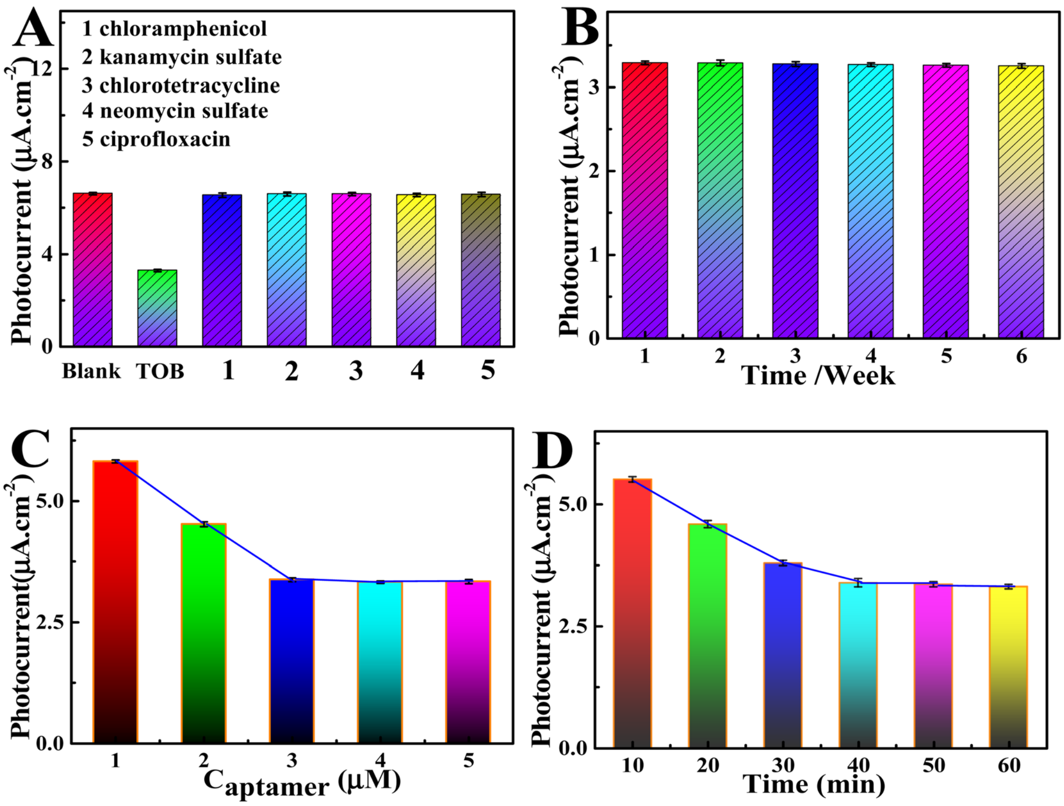

Fig. 6 (A) Selectivity and (B) stability of the PEC aptasensor, influence of different reaction parameters on the photocurrent response of the electrode. (C) Aptamer concentration, (D) incubation time of TOB with the aptamer, in 0.1 M PBS containing 0.1 M AA based on aptamer/Ti_3C_2–MoS_2/BiOI-6% for TOB detection.

6% aptasensor for detecting TOB at a concentration 0.1 ng mL^{-1} after different time intervals. The results revealed that the PEC sensor actually had a long-term shelf-life. Based on the obtained findings, the proposed PEC aptasensor seemed to exhibit the capability for detecting TOB in practical samples.

3.5. Optimization of experimental conditions for the PEC aptasensor

In order to improve the detection potential of the constructed PEC adaptive sensor, four related key parameters were optimized. Initially, with increasing aptamer concentration, the value of the photocurrent increased, but when the concentration exceeded 3.0 μM (as shown in Fig. 6C). This could be due to the fact that, at a lower concentration, aptamers can capture more targets. In contrast, high concentrations of aptamers limit the curing process due to the limited availability of active sites. Thus, 3.0 μM was selected as the optimum aptamer concentration. The binding time between TOB and the aptamer probes was subsequently studied and was found to be directly related to the strength and accuracy of the detection signal. As shown in Fig. 6D, the photocurrent stabilized within 40 min of binding time, at which point adequate reactions were achieved between TOB and the aptamer probes. Therefore, 40 min was selected as the optimal binding time for PEC sensing. It was also observed from Fig. S3C† that the photocurrent intensity increased with increasing value of the applied potential, and this could be attributed to the latter's effects on the efficiency of electron hole separation. However, when the applied potential exceeded 0.1 V, there was no further increase in the current probably because at very high applied potentials, significant background noise interferes with the sample test. Therefore, 0.1 V was selected as the best applied voltage in subsequent experiments. Finally, it was noted that the photocurrent signal gradually increased as the environment of the test solution changed from weak acid to neutral. In fact, the signal reached its highest value at pH 7.4, before subsequently decreasing at higher pH (Fig. S3D†). Thus, neutral environment was considered to be more suitable for the detection of TOB.

3.6. Real samples analysis

The concentration of TOB were detected in milk samples with the aim of proving the analysis feasibility of PEC aptasensor in real samples. As presented in Table 1, the recovery rate of TOB is 95.0–100.25%, and the RSD is 1.28–4.27%. This is basically consistent with the findings of LC-MS analysis method (the figure of HPLC-MS/MS is presented in the ESI†). It suggests that the constructed PEC aptasensor system exhibits a good practical potential.

Table 1 Determination of TOB in milk samples based on the constructed PEC sensing platform

Sample	Added (ng mL^{-1})	Found (ng mL^{-1})		Recovery (%)	RSD (%)
		PEC aptasensor	LC-MS		
1	0.1	0.095	0.097	95.00	4.27
2	1.00	0.96	0.98	96.00	2.53
3	5.00	5.01	4.98	100.20	3.31
4	10.00	9.98	9.85	99.80	1.28
5	20.00	20.05	20.11	100.25	1.34

4. Conclusion

In this study, a Ti_3C_2–MoS_2/BiOI-6% heterojunction was applied as a photovoltaic material to establish a new PEC adapter sensor for detecting TOB. The photocurrent response of the heterojunction was much higher than that of other materials, especially since it could efficiently stimulate electron transfer, enhance the efficiency of photoelectric conversion and accelerate the separation of the photo-generated electron hole pairs. The designed aptasensor also showed a wide linear range from 0.001 ng mL^{-1} to 40 ng mL^{-1} as well as excellent stability and specificity for detecting TOB. The designed optoelectronic material and PEC aptasensor can be applied to other analytes by replacing the corresponding substrate, hence offering novel thoughts for exploring biomolecules.

Conflicts of interest

There are no conflicts to declare.

References

1 X. Liu, Y. Jiang, J. Luo, X. Guo, Y. Ying, Y. Wen and Y. Wu, A SnO_2/Bi_2S_3-based photoelectrochemical aptasensor for sensitive detection of tobramycin in milk, *Food Chem.*, 2021, **344**, 128716.

2 N. H. Mukhtar, N. A. Mamat and H. H. See, Monitoring of tobramycin in human plasma via mixed matrix membrane extraction prior to capillary electrophoresis with contactless conductivity detection, *J. Pharm. Biomed. Anal.*, 2018, **158**, 184–188.

3 L. Jiang, D. Wei, K. Zeng, J. Shao, F. Zhu and D. Du, An enhanced direct competitive immunoassay for the detection of kanamycin and tobramycin in milk using multienzyme-particle amplification, *Food Analytical Methods*, 2018, **11**, 2066–2075.

4 S. Yan, X. Lai, Y. Wang, N. Ye and Y. Xiang, Label free aptasensor for ultrasensitive detection of tobramycin residue in pasteurized cow's milk based on resonance scattering spectra and nanogold catalytic amplification, *Food Chem.*, 2019, **295**, 36–41.

5 H. Siddiqui, N. Singh and R. Khan, Sensitive SERS detection of tobramycin using electrochemically synthesized silver nanoparticles, *Bull. Mater. Sci.*, 2022, **45**, 211.

6 S. Naeeminejad, K. Abnous and S. M. Taghdisi, A simple and label-free fluorescent aptasensor for detection of tobramycin: appropriate for on-site antibiotic monitoring, *Microchem. J.*, 2021, **165**, 106128.

7 J. J. Nie, L. Y. Yuan, K. Jin, X. Y. Han, Y. P. Tian and N. D. Zhou, Electrochemical detection of tobramycin based on enzymes-assisted dual signal amplification by using

a novel truncated aptamer with high affinity, *Biosen. Bioelectron.*, 2018, **122**, 254–262.

8 X. Liu, Y. N. Jiang, J. Luo, X. Y. Guo, Y. Ying, Y. Wen, H. F. Yang and Y. P. Wu, A SnO_2/Bi_2S_3-based photoelectrochemical aptasensor for sensitive detection of tobramycin in milk, *Food Chem.*, 2021, **344**, 128716.

9 L. Qiao, Y. Zhu, T. J. Zeng, Y. Y. Zhang, M. J. Zhang, K. X. Song, N. Yin, Y. N. Tao, Y. Zhao, Y. Zhang and C. Zhang, "Turn-off" photoelectrochemical aptasensor based on g-C_3N_4/WC/WO_3 composites for tobramycin detection, *Food Chem.*, 2023, **403**, 134287.

10 J. Shu, Z. Qiu, S. Lv, K. Zhang and D. Tang, Plasmonic enhancement coupling with defect-engineered TiO_{2-x}: a mode for sensitive photoelectrochemical biosensing, *Anal. Chem.*, 2018, **90**, 2425–2429.

11 L. Ge, Q. Liu, D. Jiang, L. Ding, Z. Wen, Y. Guo, C. Ding and K. Wang, Oxygen vacancy enhanced photoelectrochemical performance of Bi_2MoO_6/B, N co-doped graphene for fabricating lincomycin aptasensor, *Biosens. Bioelectron.*, 2019, **135**, 145–152.

12 M. Y. Wang, J. Z. Liu, C. Zhang, G. P. Li, B. X. Ye and L. N. Zou, A highly sensitive photoelectrochemical aptsensor based on photocathode $CuInS_2$ for the detection of tobramycin, *Microchem. J.*, 2022, **181**, 107847.

13 X. Liu, C. Wei, J. Luo, Y. Wu, X. Guo, Y. Ying, Y. Wen and H. Yang, Photoelectrochemical determination of the activity of M.SssI methyltransferase, and a method for inhibitor screening, *Microchim. Acta*, 2018, **185**, 11.

14 Y. Xu, Z. Wen, T. Wang, M. Zhang, C. Ding, Y. Guo and K. Wang, Ternary Zscheme heterojunction of Bi SPR-promoted $BiVO_4$/g-C_3N_4 with effectively boosted photoelectrochemical activity for constructing oxytetracycline aptasensor, *Biosens. Bioelectron.*, 2020, **166**, 112453.

15 J. Shu and D. Tang, Current advances in quantum-dots-based photoelectrochemical immunoassays, *Chem.–Asian J.*, 2017, **12**, 2780–2789.

16 A. B. Ganganboina, I. M. Khoris and A. Konno, CdSe-Co_3O_4@TiO_2 nanoflower–based photoelectrochemical platform probing visible light–driven virus detection, *Microchim. Acta*, 2023, **190**, 46.

17 H. Q. Chang, Q. Y. Zhu, Y. Y. Wu, A. Q. Liu, M. Jiang, C. Li, H. T. Li, L. Kong, Z. W. Chen and F. Sang, A sensitive label-free biosensor based on Ag_2S-sensitived Bi_2WO_6/BiOBr heterojunction for photoelectrochemical immunoassay of prostate specific antigen, *Talanta*, 2023, **257**, 124343.

18 Z. X. Zhang, H. Liu, L. Y. Zhai, J. H. Wu and L. Li, Construction of BiOCl-TNTs photoelectrochemical sensor for detection of hydrogen peroxide, *Chem. Phys. Lett.*, 2023, **811**, 140177.

19 R. Chen, R. Tang and C. Chen, Photoelectrochemical detection of chromium (VI) using layered MoS_2 modified BiOI, *J. Chem. Sci.*, 2020, **132**, 54.

20 L. F. Fan, G. F. Liang, C. Y. Zhang, L. Fan, W. J. Yan, Y. J. Guo, S. M. Shuang, Y. P. Bi, F. Li and C. Dong, Visible-light-driven photoelectrochemical sensing platform based on BiOI nanoflowers/TiO_2 nanotubes for detection of atrazine in environmental samples, *J. Hazard. Mater.*, 2021, **409**, 124894.

21 H. Y. Wang, Q. Z. Han, X. Ren, H. Wang, X. Kuang, D. Wu and Q. Wei, Photoelectrochemical self-powered biosensing cathodic platform by NiO nanosheets/RGO/BiOI heterostructures for detection of glucose, *J. Electroanal. Chem.*, 2020, **876**, 114497.

22 Q. Z. Han, R. Y. Wang, B. Xing, T. Zhang, M. S. Khan, D. Wu and Q. Wei, Label-free photoelectrochemical immunoassay for CEA detection based on CdS sensitized WO_3@BiOI heterostructure nanocomposite, *Biosens. Bioelectron.*, 2018, **99**, 493–499.

23 Y. Chen, Y. L. Zhou, H. S. Yin, F. Li, H. Li, R. Z. Guo, Y. H. Han and S. Y. Ai, Photoelectrochemical biosensor for histone acetyltransferase detection based on ZnO quantum dots inhibited photoactivity of BiOI nanoflower, *Sens. Actuators, B*, 2020, **307**, 127633.

24 P. C. Yan, L. Xu, X. M. Cheng, J. C. Qian, H. N. Li, J. X. Xia, Q. Zhang, M. Q. Hua and H. M. Li, Photoelectrochemical monitoring of phenol by metallic Bi self-doping BiOI composites with enhanced photoelectrochemical performance, *J. Electroanal. Chem.*, 2017, **804**, 64–71.

25 S. Chen, M. W. Tian and S. W. Liu, Novel and Selective Photoelectrochemical Sensing of Levofloxacin Based on BiOI Microflower Spheres Modified with Bi-Metal and $BiPO_4$, *Nano*, 2021, **16**(10), 2150090.

26 X. Chen, J. Zhang, J. H. Zeng, Y. X. Shi, S. Y. Lin, G. Z. Huang, H. B. Wang, Z. Kong, J. H. Xi and Z. G. Ji, MnS coupled with ultrathin MoS_2 nanolayers as heterojunction photocatalyst for high photocatalytic and photoelectrochemical activities, *J. Alloys Compd.*, 2019, **771**, 364.

27 T. N. Trung, D. B. Seo, N. D. Quang, D. J. Kim and E. T. Kim, Enhanced photoelectrochemical activity in the heterostructure of vertically aligned few-layer MoS_2 flakes on ZnO, *Electrochim. Acta*, 2018, **260**, 150.

28 J. R. Zhang, Y. Q. Zhao, L. Chen, S. F. Yin and M. Q. Cai, Density functional theory calculation on facet-dependent photocatalytic activity of MoS_2/CdS heterostructures, *Appl. Surf. Sci.*, 2019, **469**, 27.

29 S. T. Liu, X. P. Liu, J. S. Chen, C. J. Mao and B. K. Jin, Highly sensitive photoelectrochemical biosensor for microRNA159c detection based on a Ti_3C_2:CdS nanocomposite of breast cancer, *Biosens. Bioelectron.*, 2020, **165**, 112416.

30 Q. Q. Wang, L. N. Guo, W. Gao, S. F. Li, L. Hao, Z. Wang, C. Wang and Q. H. Wu, Facile synthesis of BiOI/MXene heterostructure as a superior photoelectrochemical sensor for sensitive detection of glucose, *Anal. Chim. Acta*, 2022, **1233**, 340511.

31 Z. W. Sun, Y. Tong, L. Zhao, J. Li, F. C. Gao, C. X. Wang, H. Li, L. T. Du and Y. Y. Jiang, MoS_2@Ti_3C_2 nanohybrid-based photoelectrochemical biosensor: a platform for ultrasensitive detection of cancer biomarker exosomal miRNA, *Talanta*, 2022, **238**, 123077.

32 S. S. Wua, Y. M. Su, Y. Zhu, Y. M. Zhang and M. S. Zhu, In-situ growing Bi/BiOCl microspheres on Ti_3C_2 nanosheets for upgrading visible-light-driven photocatalytic activity, *Appl. Surf. Sci.*, 2020, **520**, 146339.

33 C. Chang, L. Y. Zhu, Y. Fu and X. L. Chu, Highly active Bi/BiOI composite synthesized by one-step reaction and its capacity to degrade bisphenol A under simulated solar light irradiation, *Chem. Eng. J.*, 2013, **233**, 305.

34 X. Q. Liu, X. H. Huo, P. P. Liu, Y. F. Tang, J. Xu, X. H. Liu and Y. M. Zhou, Assembly of MoS_2 nanosheet-TiO_2 nanorod heterostructure as sensor scaffold for photoelectrochemical biosensing, *Electrochim. Acta*, 2017, **242**, 327.

35 H. C. Zhang, Y. J. Li, T. H. Xu, J. B. Wang, Z. Y. Huo, P. B. Wan and X. M. Sun, Amorphous Co-doped MoS_2 nanosheets coated on metallic CoS_2 nanocubes as an excellent electrocatalyst for hydrogen evolution, *J. Mater. Chem. A*, 2013, **3**, 15020.

36 P. V. Shinde, P. Mane, B. Chakraborty and C. S. Rout, Spinel $NiFe_2O_4$ nanoparticles decorated 2D Ti_3C_2 MXene sheets for efficient water splitting: experiments and theories, *J. Colloid Interface Sci.*, 2021, **602**, 232–241.

37 Y. Z. Bu, J. L. Xu, Y. W. Li, Q. Liu and Z. Zhang, Enhanced photocatalytic activity of BiOI under visible light irradiation by the modification of MoS_2, *RSC Adv.*, 2017, **7**, 42398.

38 H. Deng, Z. J. Li, L. Wang, L. Y. Yuan, J. H. Lan, Z. Y. Chang, Z. F. Chai and W. Q. Shi, Nanolayered Ti_3C_2 and $SrTiO_3$ Composites for Photocatalytic Reduction and Removal of Uranium(VI), *ACS Appl. Nano Mater.*, 2019, **2**, 2283–2294.